arXiv:1304.0901v1 [hep-ph] 3 Apr 2013

Centrality and $p_\perp$ dependence of J/ψ suppression in proton–nucleus collisions from parton energy loss

François Arleo,[a,b] **Rodion Kolevatov,**[c,d] **Stéphane Peigné,**[c] **Maryam Rustamova**[c]

[a]*Laboratoire Leprince-Ringuet (LLR), École polytechnique, CNRS/IN2P3 91128 Palaiseau, France*

[b]*Laboratoire d'Annecy-le-Vieux de Physique Théorique (LAPTh)*
UMR5108, Université de Savoie, CNRS, BP 110, 74941 Annecy-le-Vieux cedex, France

[c]*SUBATECH, UMR 6457, Université de Nantes, Ecole des Mines de Nantes, IN2P3/CNRS*
4 rue Alfred Kastler, 44307 Nantes cedex 3, France

[d]*Department of High Energy Physics, Saint-Petersburg State University*
Ulyanovskaya 1, 198504, Saint-Petersburg, Russia

E-mail: arleo@lapth.cnrs.fr, kolevato@subatech.in2p3.fr,
peigne@subatech.in2p3.fr, rustamov@subatech.in2p3.fr

ABSTRACT: The effects of parton energy loss and $p_\perp$-broadening in cold nuclear matter on the $p_\perp$ and centrality dependence, at various rapidities, of J/ψ suppression in p–A collisions are investigated. Calculations are systematically compared to E866 and PHENIX measurements. The very good agreement between the data and the theoretical expectations further supports $p_\perp$-broadening and the associated medium-induced parton energy loss as dominant effects in J/ψ suppression in high-energy p–A collisions. Predictions for J/ψ (and Υ) suppression in p–Pb collisions at the LHC are given.

Contents

1 Introduction

A wide range of phenomena observed in heavy-ion collisions at RHIC and LHC, both in hard and soft processes, suggests that a new, strongly interacting state-of-matter has been created, the quark-gluon plasma (QGP). One of the most striking observables is the suppression of high-$p_\perp$ particles ("jet-quenching") in A–A compared to a simple scaling of p–p collisions [1–4], which together with dijet momentum imbalance [5, 6] finds a natural explanation in parton energy loss in the QGP [7]. Another observable in heavy-ion collisions which received much attention is heavy-quarkonium suppression. Such a suppression is expected from the Debye screening of the in-medium heavy-quark potential, and was thus originally proposed as a potential signal of QGP formation (and a direct probe of the plasma temperature) [8]. However it was later realized that several other effects can modify quarkonium yields in A–A collisions (see [9] for a review), some of those effects playing a role even in absence of any hot medium.

In order to quantify the properties of the QGP created in heavy-ion collisions – a main goal of the forthcoming measurements at RHIC-II and LHC – a solid understanding

of the nuclear modification of particle spectra in cold nuclear matter is thus required. A baseline for the study is provided by p–A (or d–A) collisions where a significant suppression is already reported for some particle species. In particular, light hadron [10, 11] and J/ψ [12, 13] production in p–A collisions at forward rapidity is significantly lower than expected from the naive scaling of p–p spectra.

At the same time it is astonishing that no consensus on the cold nuclear matter effects responsible for J/ψ suppression has been achieved yet. In addition to the modifications of nuclear parton distribution functions, various mechanisms have been proposed to explain J/ψ suppression in p–A collisions. In the nucleus rest frame, a high-energy J/ψ is formed long after the nucleus thus what actually propagates through the nucleus is the parent $c\bar{c}$ pair. Some approaches attribute J/ψ suppression to an effective absorption cross section σ_{abs} of the $c\bar{c}$ pair (see Refs. [14] and [15] for recent works). Other models attribute J/ψ suppression to the increase of the $c\bar{c}$ pair invariant mass by the multiple soft rescatterings through the nucleus, leading to a reduction of the overlap with the J/ψ wave function [16] (see also [17]). In the approach used by [18] and that of our group [19], the dominant role is played by parton radiative energy loss, $i.e.$, gluon radiation induced by multiple scattering of fast partons (or color octet $c\bar{c}$ pair) travelling through the nucleus.

The present study, together with our previous works [19–21], supports parton energy loss induced by $p_\perp$-broadening as the main effect in J/ψ suppression. At this point we should stress that the physical content of our approach and that of [18], both based on parton energy loss, are actually quite different. In [18], it is assumed that the interference between gluon emissions off the incoming and outgoing parton participating to the hard production process can be neglected. Under this assumption the induced energy loss of an incoming gluon in J/ψ production is parametrically the same (up to color factors) as that of the incoming quark in the case of Drell-Yan pair production [22].

It was however argued in [21] that when the outgoing parton (or compact $c\bar{c}$ pair in the case of J/ψ production) is produced at small angle ($i.e.$, large energy E at limited $p_\perp$) in the target nucleus rest frame, the medium-induced gluon spectrum is dominated by the interference between initial and final state radiation of gluons with large formation times. Such radiation is expected in low-$p_\perp$ J/ψ production in p–A collisions, where an incoming gluon is scattered at small angle into a compact color octet $c\bar{c}$ pair. The associated energy loss is proportional to the J/ψ energy E and the role of this effect is thus expected to increase with increasing rapidity. This observation is at the basis of the energy loss scenario used in [19] to describe J/ψ suppression as a function of y (or $x_{_F}$) in a wide collision energy range for minimum bias p–A and d–A collisions. In the present study we generalize this approach to address the $p_\perp$ and centrality dependence of nuclear suppression at fixed-target (E866), RHIC and LHC energies.

The paper is organized as follows. In Section 2 we generalize the calculation scheme of [19] to address the $p_\perp$ and centrality dependence of J/ψ nuclear modification factors. Section 3 is devoted to the comparison of the model to E866 and latest PHENIX data and predictions in p–Pb collisions at the LHC are given in Section 4. Results are summarized in Section 5.

2 Model

2.1 Shift in E and $\vec{p}_\perp$

Heavy-quarkonium[1] nuclear suppression in minimum bias p–A collisions as compared to p–p collisions can be represented in terms of the ratio

$$R_{\mathrm{pA}}^{\psi}(y, p_\perp) = \frac{1}{A} \frac{\mathrm{d}\sigma_{\mathrm{pA}}^{\psi}}{\mathrm{d}y\,\mathrm{d}^2\vec{p}_\perp} \bigg/ \frac{\mathrm{d}\sigma_{\mathrm{pp}}^{\psi}}{\mathrm{d}y\,\mathrm{d}^2\vec{p}_\perp} \,, \tag{2.1}$$

where y and $\vec{p}_\perp$ are the quarkonium rapidity and transverse momentum in the c.m. frame of an elementary p–N collision (of energy $\sqrt{s}$). By convention forward (positive) rapidities correspond to the proton fragmentation region.

In the present study we generalize the model of Ref. [19] by expressing the quarkonium *double* differential cross section in p–A collisions in terms of that in p–p collisions, where a shift in the quarkonium energy E (defined in the nucleus rest frame) as in Ref. [19] but also a shift in $\vec{p}_\perp$ account, respectively, for the energy loss ε and transverse momentum broadening $\Delta\vec{p}_\perp$ of the octet $Q\bar{Q}$ pair propagating through the nucleus. The "double shift" in E and $\vec{p}_\perp$ relates the p–A and p–p double differential cross sections $\mathrm{d}\sigma/\mathrm{d}E\mathrm{d}^2\vec{p}_\perp$ as[2]

$$\frac{1}{A} \frac{\mathrm{d}\sigma_{\mathrm{pA}}^{\psi}}{\mathrm{d}E\,\mathrm{d}^2\vec{p}_\perp} = \int_\varphi \int_\varepsilon \mathcal{P}(\varepsilon, E) \frac{\mathrm{d}\sigma_{\mathrm{pp}}^{\psi}}{\mathrm{d}E\,\mathrm{d}^2\vec{p}_\perp} (E + \varepsilon, \vec{p}_\perp - \Delta\vec{p}_\perp) \;. \tag{2.2}$$

The quantity $\mathcal{P}(\varepsilon, E)$ is the energy loss probability distribution or *quenching weight* (see Section 2.2) associated to the medium-induced radiation spectrum in a target nucleus A as compared to a lighter (*e.g.*, proton) target nucleus. The integral over ε is bounded by $\varepsilon_{\max} = \min(E_{\mathrm{p}} - E, E)$, where $E_{\mathrm{p}} \simeq s/(2m_{\mathrm{p}})$ is the projectile proton energy in the nucleus rest frame. (We work in the limit $\sqrt{s} \gg m_{\mathrm{p}}$, with m_{p} the proton mass.) For the time being we consider minimum bias p–A collisions, hence the normalization factor $1/A$ in the l.h.s. of (2.2), but the model will be generalized in Section 2.5 to p–A and d–A collisions in a given centrality class. We will assume that $\Delta\vec{p}_\perp$ is uniformly distributed in the azimuthal angle φ, and has a modulus defined by (2.10).

The relation between the p–A and p–p differential cross sections in y and $\vec{p}_\perp$,

$$\frac{1}{A} \frac{\mathrm{d}\sigma_{\mathrm{pA}}^{\psi}}{\mathrm{d}y\,\mathrm{d}^2\vec{p}_\perp} = \int_\varphi \int_\varepsilon \mathcal{P}(\varepsilon, E) \left[\frac{E}{E + \varepsilon}\right] \frac{\mathrm{d}\sigma_{\mathrm{pp}}^{\psi}}{\mathrm{d}y\,\mathrm{d}^2\vec{p}_\perp} (E + \varepsilon, \vec{p}_\perp - \Delta\vec{p}_\perp) \,, \tag{2.3}$$

can be simply obtained from (2.2) by using

$$y(E, \vec{p}_\perp) = \ln\left(\frac{E}{E_{\mathrm{p}}} \frac{\sqrt{s}}{M_\perp}\right), \tag{2.4}$$

---

[1]denoted by "ψ" in the rest of the paper.

[2]The dependence of $\Delta\vec{p}_\perp$ on the azimuthal angle φ, $\Delta\vec{p}_\perp \equiv \Delta\vec{p}_\perp(\varphi)$, will be implicit in the following, and we will use the notations:

$$\int_\varphi \equiv \int \frac{\mathrm{d}\varphi}{2\pi} \;;\;\; \int_\varepsilon \equiv \int \mathrm{d}\varepsilon \;;\;\; \int_{\vec{p}_\perp} \equiv \int \mathrm{d}^2\vec{p}_\perp \text{ etc.}$$

where $M_\perp = (M^2 + p_\perp^2)^{\frac{1}{2}}$, with M the mass of the $Q\bar{Q}$ pair. In Eq. (2.3), the variable E is given by $E = E(y, \vec{p}_\perp) = E_{\mathrm{p}} e^y M_\perp / \sqrt{s}$, and the p–p cross section is evaluated at $y = y(E + \varepsilon, \vec{p}_\perp - \Delta\vec{p}_\perp)$.

For the double differential p–p cross section $\mathrm{d}\sigma_{\mathrm{pp}}/\mathrm{d}y\mathrm{d}^2\vec{p}_\perp$, we will use a parametrization consistent with the p–p data, see Section 2.3. In our model, the nuclear modification factor (2.1) obtained from (2.3) is thus fully determined by the quenching weight $\mathcal{P}(\varepsilon, E)$ and the transverse momentum broadening $\Delta p_\perp$.

2.2 Quenching weight and $\Delta p_\perp$

In Ref. [19] the appropriate medium-induced gluon radiation spectrum $\mathrm{d}I/\mathrm{d}\omega$ in quarkonium production in p–A collisions (as compared to p–B collisions) was derived, as well as the associated quenching weight $\mathcal{P}(\varepsilon, E)$,

$$\mathcal{P}(\varepsilon, E) = \frac{\mathrm{d}I}{\mathrm{d}\varepsilon} \exp\left\{ -\int_\varepsilon^\infty \mathrm{d}\omega \frac{\mathrm{d}I}{\mathrm{d}\omega} \right\}, \tag{2.5}$$

$$\frac{\mathrm{d}I}{\mathrm{d}\omega} = \frac{N_c\,\alpha_s}{\omega\,\pi} \left\{ \ln\left(1 + \frac{\ell_{\perp\mathrm{A}}^2 E^2}{M_\perp^2 \omega^2}\right) - \ln\left(1 + \frac{\Lambda_\mathrm{B}^2 E^2}{M_\perp^2 \omega^2}\right) \right\} \Theta(\ell_{\perp\mathrm{A}}^2 - \Lambda_\mathrm{B}^2), \tag{2.6}$$

where $\ell_{\perp\mathrm{A}}$ represents the accumulated transverse momentum transfer due to soft rescatterings in the target nucleus A, and $\Lambda_\mathrm{B} = \max(\Lambda_{\mathrm{QCD}}, \ell_{\perp\mathrm{B}})$. The latter dependence on Λ_{QCD} arises from vetoing induced gluon radiation with $k_\perp < \Lambda_{\mathrm{QCD}}$ [19]. Note that $\mathcal{P}(\varepsilon, E)$ is determined analytically in terms of the dilogarithm function $\mathrm{Li}_2(x)$,

$$\mathcal{P}(\varepsilon, E) = \frac{\mathrm{d}I}{\mathrm{d}\varepsilon} \exp\left\{ -\frac{N_c\,\alpha_s}{2\pi} \left[\mathrm{Li}_2\left(-\frac{\Lambda_\mathrm{B}^2 E^2}{M_\perp^2 \varepsilon^2}\right) - \mathrm{Li}_2\left(-\frac{\ell_{\perp\mathrm{A}}^2 E^2}{M_\perp^2 \varepsilon^2}\right) \right] \right\}. \tag{2.7}$$

The *semi-hard* transfer $\ell_{\perp\mathrm{A}}$ is given by

$$\ell_{\perp\mathrm{A}}^2 = \hat{q}_\mathrm{A}\, L_\mathrm{A}, \tag{2.8}$$

where L_A is the *effective* path length[3] across the target nucleus A and $\hat{q}_\mathrm{A}$ the transport coefficient [19]

$$\hat{q}_\mathrm{A} = \hat{q}(x_\mathrm{A}) \equiv \hat{q}_0 \left(\frac{10^{-2}}{x_\mathrm{A}}\right)^{0.3}; \quad x_\mathrm{A} = \min(x_{0\mathrm{A}}, x_2); \quad x_{0\mathrm{A}} \equiv \frac{1}{2m_\mathrm{p}L_\mathrm{A}}; \quad x_2 = \frac{M_\perp}{\sqrt{s}}e^{-y}. \tag{2.9}$$

The parameter $\hat{q}_0 = 0.075\,\mathrm{GeV}^2/\mathrm{fm}$ was extracted in Ref. [19] from a fit to the E866 data for $R_{\mathrm{W/Be}}^{\mathrm{J}/\psi}$. We will use this value in the present study, which thus contains no free parameter.[4]

---

[3]For the present study we will use $L_{\mathrm{Be}} = 3.24\,\mathrm{fm}$, $L_{\mathrm{Fe}} = 6.62\,\mathrm{fm}$, $L_\mathrm{W} = 9.35\,\mathrm{fm}$, $L_{\mathrm{Au}} = 10.23\,\mathrm{fm}$ and $L_{\mathrm{Pb}} = 10.11\,\mathrm{fm}$ for minimum bias collisions, as well as $L_\mathrm{p} = 1.5\,\mathrm{fm}$ [19]. The dependence of L_{Au} (resp. L_{Pb}) on the centrality class in d–Au collisions at RHIC (resp. p–Pb collisions at LHC) is described in Section 2.5, see Table 2, and in Appendix B.

[4]Let us also note that in the fitting procedure of Ref. [19], small values of $\hat{q}_0$ and thus of $\hat{q}L$ were explored, for which the dependence of (2.6) on Λ_{QCD} is relevant. However, it turns out that the extracted $\hat{q}_0 = 0.075\,\mathrm{GeV}^2/\mathrm{fm}$ is large enough to satisfy $\sqrt{\hat{q}L} > 0.25\,\mathrm{GeV}$ for all values of L_A (including L_p) and x_2 considered in the present study, as can be easily checked from (2.9) using $L_\mathrm{p} = 1.5\,\mathrm{fm}$. The present study is thus independent of the value of Λ_{QCD} provided $\Lambda_{\mathrm{QCD}} \leq 0.25\,\mathrm{GeV}$.

Finally, the transverse momentum broadening in p–A with respect to p–B collisions is simply given by

$$(\Delta \vec{p}_\perp)^2 = \ell_{\perp \mathrm{A}}^2 - \ell_{\perp \mathrm{B}}^2 = \hat{q}_\mathrm{A} L_\mathrm{A} - \hat{q}_\mathrm{B} L_\mathrm{B} \,. \tag{2.10}$$

In our study we neglect the fluctuations of the broadening $\ell_\perp^2$ around the average value $\hat{q}L$. We have checked that assuming a distribution in $\ell_\perp$ of the Gaussian type, $P(\ell_\perp) \propto \exp\left(-\ell_\perp^2/\hat{q}L\right)$, only slightly modifies (by at most 10%) the predictions for $R_{\mathrm{pA}}^\psi(y, p_\perp)$ presented in Sections 3 and 4, without changing the overall shape of R_{pA}.

2.3 Parametrization of the p–p cross section

Similarly to Ref. [19], we use for the double differential p–p cross section $\mathrm{d}\sigma_{\mathrm{pp}}/\mathrm{d}y\mathrm{d}^2\vec{p}_\perp$ a simple parametrization consistent with the available p–p data, rather than relying on some model-dependent quarkonium production mechanism in hadronic collisions.

The double differential cross section of prompt J/ψ and Υ production can be conveniently parametrized as

$$\frac{\mathrm{d}\sigma_{\mathrm{pp}}^\psi}{\mathrm{d}y\,\mathrm{d}^2\vec{p}_\perp} = \mathcal{N} \times \left(\frac{p_0^2}{p_0^2 + p_\perp^2}\right)^m \times \left(1 - \frac{2M_\perp}{\sqrt{s}} \cosh y\right)^n \equiv \mathcal{N} \times \mu(p_\perp) \times \nu(y, p_\perp) \,. \tag{2.11}$$

At the LHC ($\sqrt{s} = 7$ TeV) the values of the free parameters $\mathcal{N}$, p_0, m and n are obtained from a global fit of ALICE [23], ATLAS [24] and LHCb [25] data on prompt J/ψ production[5] and from a fit of LHCb data [26] on Υ production. They are summarized in Table 1 together with the corresponding χ^2/ndf values.[6]

Quarkonium	$\sqrt{s}$ (GeV)	p_0 (GeV)	n	m	χ^2/ndf
J/ψ	7000	4.2	19.2	3.5	54/139
Υ	7000	6.6	13.8	2.8	48/72
J/ψ	200	3.3	(8.3)	4.3	27/37
J/ψ	38.7	3.1	(4.5)	5.3	45/19

Table 1. Values of the fit parameters obtained from a fit to LHC (J/ψ and Υ), PHENIX, and E789 p–p data. Values given in parenthesis are fixed in the fitting procedure (see text for details).

At RHIC the amount and precision of data are not sufficient to fix precisely the fit parameters. The fit to the double differential data measured by PHENIX [27] is therefore performed by fixing the value of $n = 8.3$ obtained from the fit of the single differential cross section $\mathrm{d}\sigma_{\mathrm{pp}}^{J/\psi}/\mathrm{d}y$, see Ref. [19].

Finally, a fit to the J/ψ E789 ($\sqrt{s} = 38.7$ GeV) data [28] is also performed with the aim to compare the model predictions to the E866 data [12] at the same center-of-mass energy.[7] Like at RHIC, the number of fit parameters is reduced by fixing the value of $n = 4.5$ obtained from fitting $\mathrm{d}\sigma_{\mathrm{pp}}^{J/\psi}/\mathrm{d}x_F$ data at this energy [19].

---

[5]The ALICE data are only given for *inclusive* J/ψ production, *i.e.* including J/ψ from B-decays.

[6]The value of $\mathcal{N}$ is irrelevant as we consider only cross section *ratios* and is therefore not given.

[7]Note however that the E789 data have been taken at $x_F = 0$ only. Therefore this parametrization may not be valid at large x_F for which the model is compared to the E866 measurements, see Section 3.1.
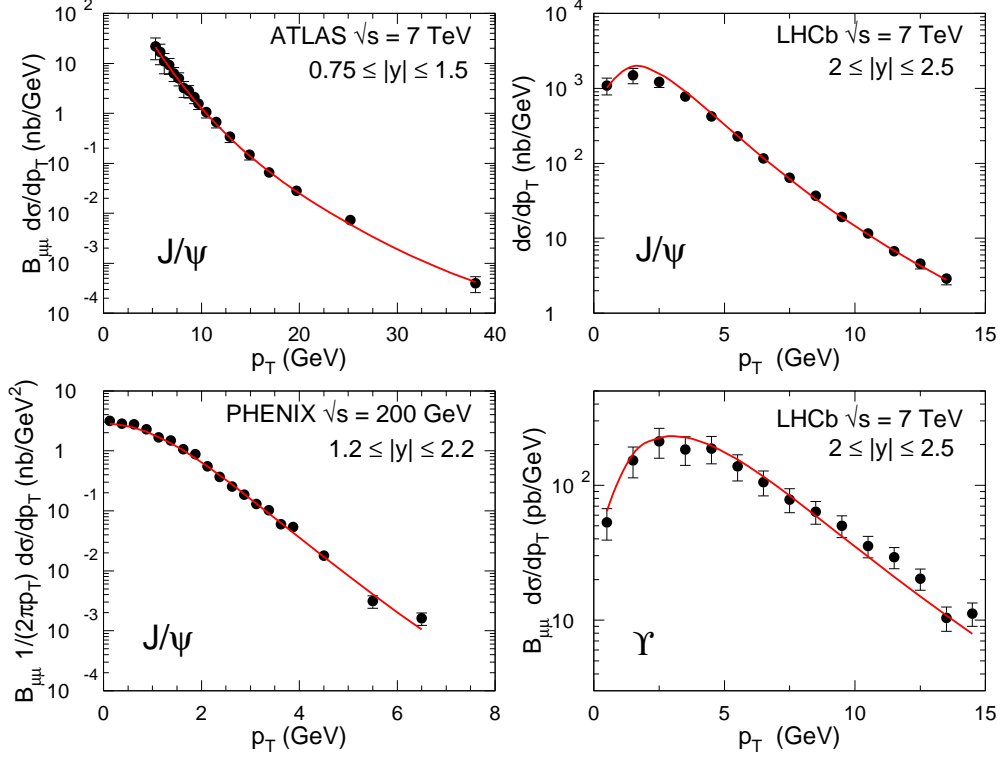
Figure 1. Comparison between heavy-quarkonium (J/ψ, Υ) production data in p–p collisions and the parametrization (2.11) (solid red line). Data are taken from ATLAS [24], LHCb [25, 26], and PHENIX [27].

The agreement between some of the prompt J/ψ and Υ measurements at RHIC and LHC and the parametrization (2.11) is shown in Fig. 1. Finally, let us mention that the functional form of the parametrization (2.11) is fully consistent with that for the single differential rate in x_F used in [19], as we briefly show in Appendix A.

2.4 A useful approximation for $R_{\mathrm{pA}}^{\psi}(y, p_\perp)$

Using (2.3) and (2.11) the attenuation factor (2.1) reads

$$
\begin{aligned}
R_{\mathrm{pA}}^{\psi}(y, p_\perp) &= \int_\varphi \int_\varepsilon \mathcal{P}(\varepsilon, E) \left[\frac{E}{E+\varepsilon} \right] \frac{\mu(|\vec{p}_\perp - \Delta\vec{p}_\perp|)}{\mu(p_\perp)} \frac{\nu(E+\varepsilon, \vec{p}_\perp - \Delta\vec{p}_\perp)}{\nu(E, p_\perp)} \\
&= \int_\varepsilon \mathcal{P}(\varepsilon, E) \left[\frac{E}{E+\varepsilon} \right] \frac{\nu(E+\varepsilon, p_\perp)}{\nu(E, p_\perp)} \int_\varphi \frac{\mu(|\vec{p}_\perp - \Delta\vec{p}_\perp|)}{\mu(p_\perp)} \frac{\nu(E+\varepsilon, \vec{p}_\perp - \Delta\vec{p}_\perp)}{\nu(E+\varepsilon, p_\perp)} .
\end{aligned}
\tag{2.12}
$$

Since $\mathcal{P}(\varepsilon, E)$ is peaked at small values of ε, we neglect ε in the latter φ integral. In this approximation, the φ and ε integrals factorize,

$$
R_{\mathrm{pA}}^{\psi}(y, p_\perp) \simeq R_{\mathrm{pA}}^{\mathrm{broad}}(y, p_\perp) \cdot R_{\mathrm{pA}}^{\mathrm{loss}}(y, p_\perp) ,
\tag{2.13}
$$

where

$$R_{\text{pA}}^{\text{broad}}(y, p_\perp) \equiv \int_\varphi \frac{\mu(|\vec{p}_\perp - \Delta\vec{p}_\perp|)}{\mu(p_\perp)} \frac{\nu(E, \vec{p}_\perp - \Delta\vec{p}_\perp)}{\nu(E, p_\perp)}, \qquad (2.14)$$

$$R_{\text{pA}}^{\text{loss}}(y, p_\perp) \equiv \int_\varepsilon \mathcal{P}(\varepsilon, E) \left[\frac{E}{E + \varepsilon}\right] \frac{\nu(E + \varepsilon, p_\perp)}{\nu(E, p_\perp)}. \qquad (2.15)$$

The factor $R_{\text{pA}}^{\text{broad}}(y, p_\perp)$ describes nuclear modification due to transverse momentum broadening only, as can be seen by setting $\mathcal{P}(\varepsilon, E) = \delta(\varepsilon)$ in (2.12). The factor $R_{\text{pA}}^{\text{loss}}(y, p_\perp)$ describes the effect of energy loss only, obtained by setting $\Delta p_\perp = 0$ in (2.12). In the following we will use the factorized expression (2.13), which turns out to be a very accurate approximation to (2.1) in all the practical applications of Sections 3 and 4.

Finally, let us mention that the $p_\perp$-inclusive nuclear suppression factor $R_{\text{pA}}^\psi(y)$ studied in Ref. [19] can be simply recovered from (2.12), along the same lines as in Appendix A where the parametrization of $d\sigma_{\text{pp}}/dy$ is obtained from $d\sigma_{\text{pp}}/dyd^2\vec{p}_\perp$. Integrating both the numerator and denominator of (2.1) (and thus of (2.12)) over $\vec{p}_\perp$, the function $\nu(y, p_\perp)$ can be replaced by its value at a typical $\bar{p}_\perp$ determined by the width of $\mu(p_\perp)$ (see (A.6)), and the $\vec{p}_\perp$-integral of $\mu(p_\perp)$ cancels between the numerator and denominator. As a result, the $p_\perp$-inclusive suppression factor reads $R_{\text{pA}}^\psi(y) \simeq R_{\text{pA}}^{\text{loss}}(y, \bar{p}_\perp)$, which corresponds exactly to the quantity studied in Ref. [19].

2.5 Centrality dependence

In the preceding sections we addressed the case of minimum bias p–A collisions. The model is generalized to the case of p–A collisions at a given centrality (or at a given impact parameter b) by using the effective length L_{A} corresponding to that centrality. Since L_{A} fully determines the essential quantities $\ell_{\perp\text{A}}$ and $\Delta p_\perp$ of the model (see (2.8), (2.9) and (2.10)), this is the only modification required. However, the impact parameter (as well as the number of participants) is not a direct experimental observable, and the consistent way for making a theoretical estimate of L_{A} is to follow the experimental procedure as closely as possible.

Both at RHIC [29] and the LHC [30] a centrality selection is done by triggering on event multiplicity in forward detectors. This multiplicity is strongly correlated with the number of participating nucleons from the target nucleus. Thus, multiplicity cuts impose a restriction on the number of participants in a given event. The values of the forward event multiplicities which separate centrality classes in the experiment are chosen to attribute a certain fraction of the total inelastic cross section to each centrality class. The common choice is making 20% slices from the most central (largest multiplicity) to the peripheral (lowest multiplicity) events. The exception is the most peripheral class which is taken at 60–88% of the total inelastic cross section at RHIC (class D) and 60-100% at the LHC (class 4).

To compute the average path length L_{A} for each centrality class, we employ the following procedure.

First, we define centrality classes in terms of the number of participants N_{p}. Within a Glauber description (see Appendix B.1), we define a centrality class by the threshold

Glauber, RHIC					Glauber, LHC				
class	$N_p^{\min}$; $N_p^{\max}$	$\frac{P(\text{class})}{P(N \geq 1)}$	$\langle N_c \rangle$	L_{Au}	class	$N_p^{\min}$; $N_p^{\max}$	$\frac{P(\text{class})}{P(N \geq 1)}$	$\langle N_c \rangle$	L_{Pb}
A	11; 197	0.28	15.9	12.87	1	12; 208	0.246	14.8	13.46
B	8; 12	0.24	10.9	9.62	2	9; 12	0.215	10.5	9.55
C	5; 8	0.23	7.0	7.17	3	5; 8	0.215	6.5	6.29
D	2; 4	0.29	3.6	3.84	4	1; 5	0.428	2.4	3.39

Table 2. Average number of binary collisions $\langle N_c \rangle$, and average path length L_A (in fm) for different centrality classes (A–D at RHIC and 1–4 at LHC), as obtained in a Glauber calculation. See text and Appendix B for details.

values $N_p^{\min}$ and $N_p^{\max}$ of N_p which saturate approximately the same fraction of the total interaction probability $P(N_p \geq 1) = 1$ as the fraction of the total inelastic cross section attributed to the centrality classes in the experimental selection procedure. We note however that centrality in the experiment is defined in terms of event multiplicity rather than N_p. In a given multiplicity class one may have events where N_p is slightly above or below the thresholds defined according to a sharp cut on the fraction of the total interaction probability as a function of N_p. In order to account for this possibility we widen the N_p interval attributed to each class and use the new threshold values in further estimates. Those values are given in Table 2. As a consistency check of our class selection method, we calculate the average number of binary collisions $\langle N_c \rangle$ for the different centrality classes. These numbers coincide with the results of the Glauber Monte-Carlo supplemented with the p–p RHIC data used by the PHENIX collaboration (see Table 1 in Ref. [13]).

Second, within each of the centrality classes defined in such a way, we determine, also in the Glauber model, the average number of target nucleons participating in the rescattering of the fast color octet $Q\bar{Q}$ pair, see Appendix B.2. The average path length L_A for a given centrality class directly follows from this number. Table 2 displays the values of L_{Au} (RHIC) and L_{Pb} (LHC) to be used in our model, for each centrality class.

3 Comparison to E866 and RHIC data

The J/ψ nuclear production ratio is computed as a function of $p_\perp$ for various values of y or $x_F = (2M_\perp/\sqrt{s}) \sinh y$. The only parameter of the model, the transport coefficient $\hat{q}_0$, has been fixed to $\hat{q}_0 = 0.075$ GeV^2/fm in [19] from the x_F dependence of J/ψ suppression measured in p–W collisions by E866 [12]. In the numerical calculations we use $\Lambda_{\text{QCD}} = 0.25$ GeV (however see footnote 4), $\alpha_s = 0.5$, and $M = 3$ GeV ($M = 9$ GeV) for the mass of the $c\bar{c}$ ($b\bar{b}$) pair.

3.1 E866

The E866 collaboration has measured the J/ψ suppression in p–Fe and p–W collisions (with respect to p–Be) at $\sqrt{s} = 38.7$ GeV as a function of the transverse momentum for three domains in x_F [12]. At small x_F, J/ψ production can be affected by nuclear absorption since the typical J/ψ hadronization time becomes comparable to (or less than) the size of the nuclear targets [19]. The model is therefore compared to the E866 data

in the intermediate-x_F ($0.2 \leq x_F \leq 0.6$, $\langle x_F \rangle = 0.308$) and large-$x_F$ ($0.3 \leq x_F \leq 0.93$, $\langle x_F \rangle = 0.48$) domains.
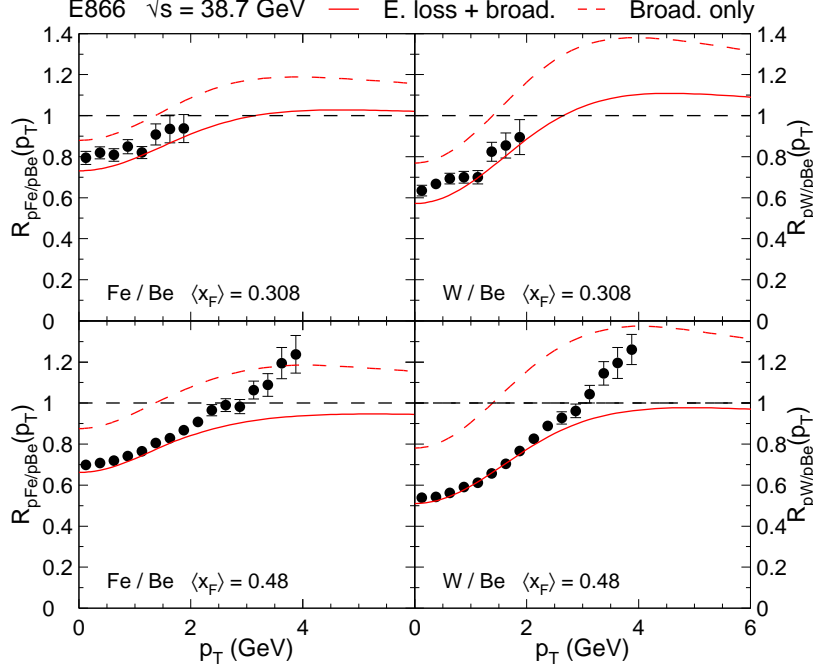

Figure 2. Model predictions (solid red curves) for the J/ψ nuclear suppression factor compared to the E866 data for $R_{\mathrm{Fe/Be}}(p_\perp)$ (left) and $R_{\mathrm{W/Be}}(p_\perp)$ (right), in the intermediate-x_F ($\langle x_F \rangle = 0.308$, top) and large-$x_F$ ($\langle x_F \rangle = 0.48$, bottom) ranges. The dashed lines indicate the effect of momentum broadening only, $R_{\mathrm{pA}}^{\mathrm{broad}}(y, p_\perp)$, Eq. (2.14).

In Fig. 2 are shown as solid lines the Fe/Be (left) and W/Be (right) nuclear production ratios at intermediate (top) and large (bottom) x_F. The ratio $R_{\mathrm{pA}}(p_\perp)$ increases with $p_\perp$ in almost the whole $p_\perp$ range, with more pronounced suppression (at $p_\perp = 0$ GeV, where R_{pA} is the smallest) in W targets and at large x_F. The $p_\perp$ dependence essentially arises from that of $R_{\mathrm{pA}}^{\mathrm{broad}}(p_\perp)$, shown as dashed lines. The sole energy loss effect, $R_{\mathrm{pA}}^{\mathrm{loss}}(y, p_\perp)$, proves rather flat in this $p_\perp$-domain, but is essential to fix the magnitude of R_{pA}, leading to a remarkable agreement between the data and the model predictions in the $0 \leq p_\perp \leq 2$ GeV range.

At large x_F, the data overshoot the theoretical expectations above $p_\perp \gtrsim 3$ GeV, for which the model predictions flatten out. Several reasons might explain this disagreement. First of all, the parametrization of the p–p cross section (using E789 data, see Section 2.3) has been performed at $x_F = 0$ only; it could therefore well be that this fit, used to compute R_{pA}, is no longer appropriate to describe the p–p production cross section at both large $x_F \simeq 0.4$ *and* $p_\perp \gtrsim 3$ GeV. Also note that the theoretical calculations have been performed at $x_F = \langle x_F \rangle$ while the data are averaged on a rather large x_F-bin. When $p_\perp$ gets larger, the kinematical correlation between $p_\perp$ and x_F would therefore tend to decrease the typical

x_F, for which the model would predict slightly larger R_{pA} ratios.[8] For those reasons it is difficult to draw any firm conclusion from the comparison between the model and the E866 data at large x_F and $p_\perp$.

Putting aside the latter $(p_\perp, x_F)$ region, it is remarkable that the model reproduces quantitatively the $p_\perp$ dependence of J/ψ suppression in various nuclei and at different x_F values. The fact that the *same* quantity, $\hat{q}L$, determines the strength of medium-induced gluon radiation (and therefore energy loss) necessary to explain the x_F dependence of R_{pA} (see Ref. [19]) and the amount of momentum broadening required in the present study to reproduce the shape of R_{pA} as a function of $p_\perp$, strongly supports parton energy loss induced by momentum broadening as the dominant effect in quarkonium nuclear suppression.

3.2 RHIC

Let us now move to RHIC energy, where the $p_\perp$ dependence of J/ψ suppression in d–Au collisions has been reported recently by the PHENIX collaboration [13].

In Fig. 3 the model predictions are compared to the PHENIX data measured in minimum bias d–Au collisions, at backward $(-2.2 \leq y \leq -1.2$, left), central $(|y| \leq 0.35$, middle) and forward $(1.2 \leq y \leq 2.2$, right) rapidities.[9] The model reproduces the trend seen in data, namely an increase with $p_\perp$ up to $p_\perp \simeq 4$–5 GeV. Around those values, some nuclear enhancement, $R_{pA}(p_\perp) > 1$, is visible at backward and central rapidities, but would need more precise data to be confirmed. At forward rapidity, the suppression due to energy loss is too strong to observe such an enhancement, both in the data and in the model. As for the results at E866 energy discussed earlier, the $p_\perp$ shape of $R_{pA}(p_\perp)$ is essentially driven by the effect of momentum broadening, Eq. (2.14), shown as dashed lines.

On top of minimum bias collisions, J/ψ suppression has also been measured in four centrality classes of d–Au collisions (0–20%, 20–40%, 40–60%, 60–88%). The data are shown in Fig. 4 for the three rapidity bins and four centrality classes and compared to the model. Details on the medium length L corresponding to the various centrality classes of d–Au collisions and used in the theoretical calculation can be found in Section 2.5 and Appendix B. As for minimum bias collisions, the model predictions prove in very good agreement with data. In particular, the centrality dependence is well reproduced by the model, with rather pronounced effects in the 0–20% most central collisions, and almost negligible effects, $R_{pA} \simeq 1$ in the whole $p_\perp$-range for the 60–88% most peripheral collisions.

Therefore it appears that the present model, based on parton energy loss and momentum broadening, offers a better agreement on the $p_\perp$ and centrality dependence of R_{pA} than models based purely on modification of parton densities [15] and nuclear absorption [14] which tend to predict a flatter dependence of $R_{pA}(p_\perp)$.

---

[8]We checked that averaging properly over the whole x_F-range considered experimentally increases by $\sim 5\%$ the R_{pA} ratios at large $p_\perp$, therefore slightly reducing the discrepancy with experimental data.

[9]Calculations are performed at the fixed values of $y = -1.7$, 0, $+1.7$ respectively. We checked that similar results are obtained when averaging over the experimental y range. Note also that for $y = -1.7$, the J/ψ hadronization time is comparable to the size of the gold nucleus, and nuclear absorption may play a role [19].
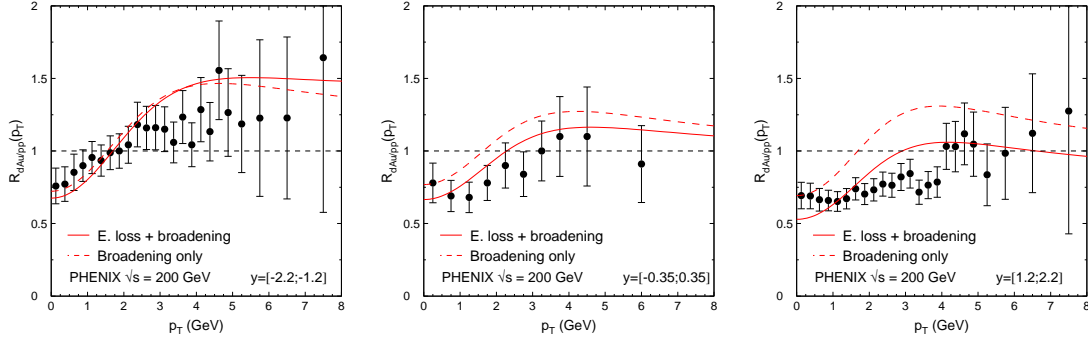
Figure 3. Model predictions for the J/ψ nuclear suppression factor $R_{\mathrm{pA}}(p_\perp)$ in minimum bias d–Au collisions at RHIC, at backward (left), central (middle) and forward (right) rapidities (solid curves). The dashed lines indicate the effect of momentum broadening only, $R_{\mathrm{pA}}^{\mathrm{broad}}(y, p_\perp)$, Eq. (2.14).
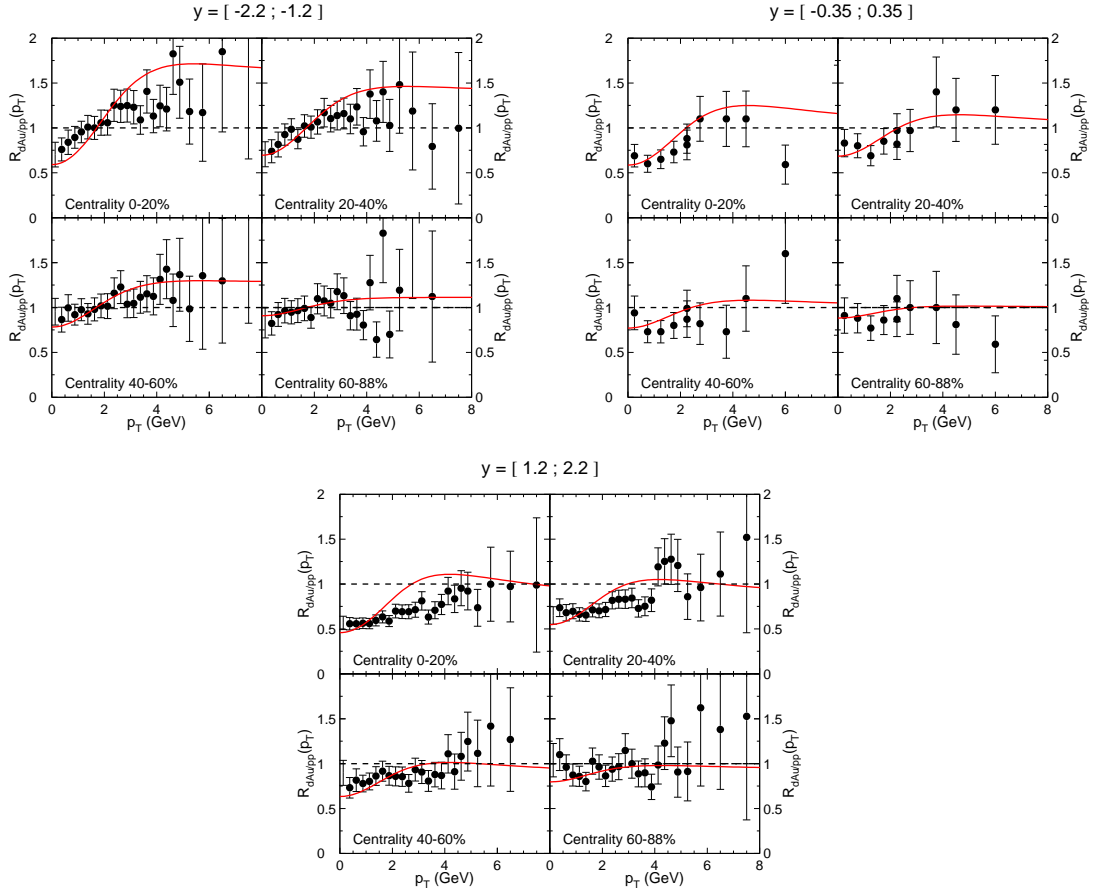

Figure 4. Same as Fig. 3 in the four centrality classes (from top left to bottom right in each panel) at backward, central and forward rapidities (upper left, upper right, bottom).

4 Predictions for p–Pb collisions at the LHC

A run of p–Pb collisions at $\sqrt{s} = 5$ TeV has taken place at LHC early 2013 with an integrated luminosity of $\mathcal{L} \simeq 30$ nb^{-1} collected by ALICE, ATLAS and CMS experiments. This will allow for precise measurements of J/ψ and Υ production in p–A collisions at an unprecedented energy, on a wide range of rapidities ($|y| < 5$) and transverse momenta, and consequently clarify the role of cold nuclear matter effects at high energy. In this section, we therefore provide predictions for J/ψ and Υ nuclear production ratios R_{pA} as a function of $p_\perp$, for different rapidities ($y = -3.7, 0, 2.8$)[10] and centrality classes (labelled $1 \ldots 4$ from central to peripheral collisions, see Section 2.5 for details).

In Fig. 5 we show the J/ψ nuclear production ratio for minimum bias p–Pb collisions, from backward (left) to central (middle) and forward (right) rapidities. At all rapidities a depletion of J/ψ production is expected at low $p_\perp$, say $p_\perp \lesssim 3$ GeV. At larger $p_\perp$ a "Cronin peak" might only be visible at large rapidity, $y = 2.8$ and above, in minimum bias collisions. Quite generally the effects of both energy loss and momentum broadening are expected to become more pronounced at larger rapidities. As shown in [19], energy loss effects prove stronger at large positive rapidity because of the energy dependence of the average energy loss, $\Delta E \propto E$, associated to the medium-induced spectrum (2.6).
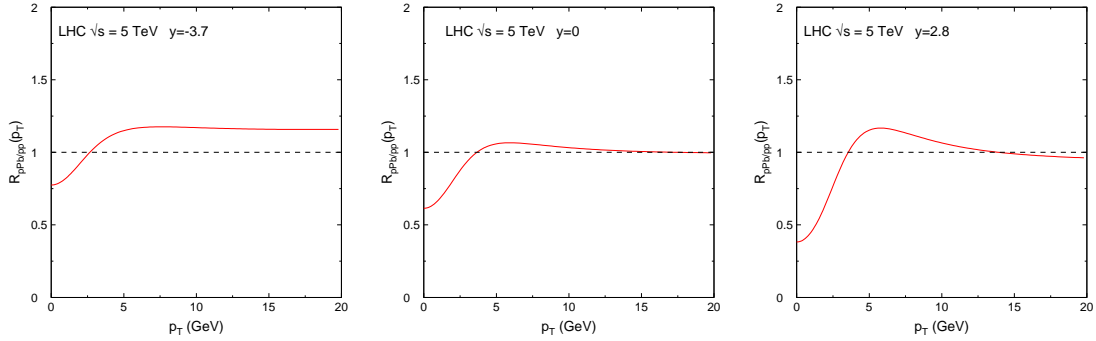

Figure 5. Prediction for the J/ψ nuclear suppression factor $R_{\mathrm{pA}}(p_\perp)$ in minimum bias p–Pb collisions at LHC, for backward, central and forward rapidities.

The model predictions are also provided in the four centrality classes of p–Pb collisions in Fig. 6. As expected the deviations of R_{pA} from unity are largest in the most central collisions, while in the most peripheral p–Pb collisions (centrality class 4), $R_{\mathrm{pA}}(p_\perp) \simeq 1$ at all $p_\perp \gtrsim 2$–3 GeV. The most spectacular effects can be seen in the central collisions (class 1) and at forward rapidity, where $R_{\mathrm{pA}} \simeq 0.25$ at $p_\perp = 0$ GeV and $R_{\mathrm{pA}} \simeq 1.3$ at $p_\perp = 6$ GeV.

---

[10] Here the rapidity y is defined in the center-of-mass frame of the proton–nucleon collision, related to the rapidity in the laboratory frame y_{lab} as $y = y_{\mathrm{lab}} - 0.465$ in p–Pb collisions and $y = y_{\mathrm{lab}} + 0.465$ in Pb–p collisions. The value $y = 2.8$ (respectively $y = -3.7$) is chosen to correspond to the median rapidity of the ALICE spectrometer acceptance, namely $2.5 < y_{\mathrm{lab}} < 4$, in p–Pb (respectively Pb–p) collisions.
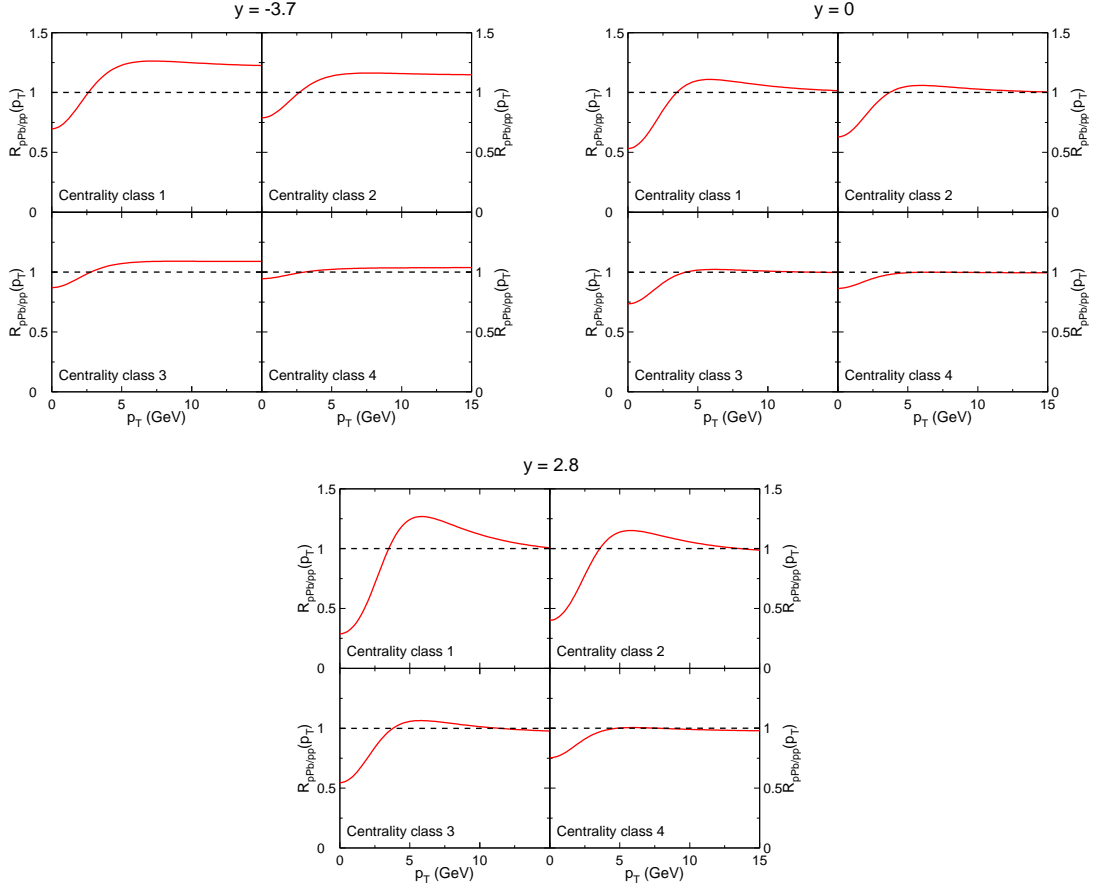
Figure 6. Same as Fig. 5 in the four centrality classes (from top left to bottom right in each panel) at backward, central and forward rapidities (upper left, upper right, bottom).

Predictions are performed as well in the Υ channel. The expected $R_{\rm pA}^{\Upsilon}$ at the LHC is shown in Fig. 7 for the most central p–Pb collisions (centrality class 1). Because of the mass dependence of the energy loss, $\Delta E \propto M_{\perp}^{-1}$, the suppression due to energy loss, $R_{\rm pA}^{\rm loss}$, is milder than for J/ψ. Moreover, although the amount of momentum broadening experienced by J/ψ and Υ states is expected to be similar (neglecting the x dependence of the transport coefficient), the height of the Cronin peak is much less pronounced for Υ than for J/ψ (compare *e.g.* Fig. 6 bottom and Fig. 7 right).[11] This is due to the flatter Υ $p_{\perp}$-spectrum as compared to that of J/ψ production, see Fig. 1 and the values of the parameters p_0 and m in Table 1. As can be seen in Fig. 7, Υ suppression, $R_{\rm pA}^{\Upsilon} < 1$, is predicted in the range $0 \leq p_{\perp} \leq 6$ GeV at mid-rapidity. The suppression extends to larger $p_{\perp}$ than for J/ψ due to the larger value of the p_0 parameter in the p–p cross section. The suppression is maximal at $p_{\perp} = 0$ GeV, where $R_{\rm pA}^{\Upsilon} \simeq 0.85$ (resp. 0.65) at $y = 0$ (resp. $y = 2.8$).

---

[11]As a matter of fact, the slight enhancement arising from $R_{\rm pA}^{\rm broad}$ is compensated by energy loss effects, $R_{\rm pA}^{\rm loss} < 1$, making $R_{\rm pA}^{\Upsilon}$ smaller than one at all $p_{\perp}$.
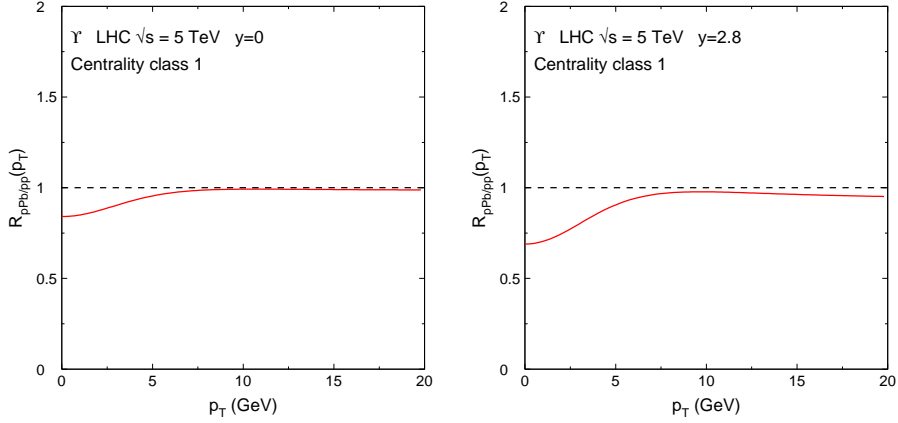
Figure 7. Predictions for the Υ nuclear suppression factor $R_{\mathrm{pA}}(p_\perp)$ in central p–Pb collisions (centrality class 1) at LHC, for central (left) and forward (right) rapidities.

5 Conclusion

Following our earlier work [19], we studied the effects of parton $p_\perp$-broadening and energy loss in cold nuclear matter on the $p_\perp$ dependence of J/ψ and Υ suppression in p–A collisions. We found that the momentum broadening is responsible for the fast variation of J/ψ suppression with $p_\perp$, while medium-induced energy loss essentially affects the magnitude of R_{pA}.

Using the transport coefficient $\hat{q}_0 = 0.075$ GeV^2/fm fixed in [19], the model predictions prove in very good agreement with recent PHENIX data [13] in minimum bias and centrality-dependent d–Au collisions at $\sqrt{s} = 200$ GeV. Our results are also successfully compared to earlier results from the E866 collaboration [12]. Finally, predictions for J/ψ and Υ suppression in p–Pb collisions (minimum bias and in four centrality classes) at the LHC ($\sqrt{s} = 5$ TeV) are provided.

The good description, within a consistent framework, of both the rapidity and transverse momentum dependence of $R_{\mathrm{pA}}^{\mathrm{J}/\psi}$ from fixed-target experiments to RHIC is a hint that parton energy loss induced by momentum broadening might be the dominant effect responsible for J/ψ suppression in p–A collisions.

Acknowledgments

A Fits of p–p single and double differential rates

Here we compare the parametrization (2.11) for the double differential p–p cross section used in the present study and that for the single differential rate $\mathrm{d}\sigma_{\mathrm{pp}}/\mathrm{d}x_F$ used in [19],

$$\frac{\mathrm{d}\sigma_{\mathrm{pp}}^{\psi}}{\mathrm{d}x_F} \propto \frac{(1-x')^n}{x'}\,, \tag{A.1}$$

where the variables x_F and x' are defined by

$$x_F = \frac{E}{E_{\mathrm{p}}} - \frac{E_{\mathrm{p}}}{E}\frac{M_{\perp}^2}{s} = \frac{2M_{\perp}}{\sqrt{s}}\,\sinh y\,, \tag{A.2}$$

$$x' = \frac{E}{E_{\mathrm{p}}} + \frac{E_{\mathrm{p}}}{E}\frac{M_{\perp}^2}{s} = \frac{2M_{\perp}}{\sqrt{s}}\,\cosh y\,. \tag{A.3}$$

Eq. (A.1) translates in rapidity to (use $\partial x_F/\partial y = x'$)

$$\frac{\mathrm{d}\sigma_{\mathrm{pp}}^{\psi}}{\mathrm{d}y} \propto (1-x')^n = \left(1 - \frac{2M_{\perp}}{\sqrt{s}}\cosh y\right)^n = \nu(y,p_{\perp})\,. \tag{A.4}$$

In Ref. [19] no information on $p_{\perp}$-distributions was used, and $p_{\perp}$ was replaced by some typical value, assumed to be $\bar{p}_{\perp} = 1\,\mathrm{GeV}$.

In the present study, the single differential cross section $\mathrm{d}\sigma_{\mathrm{pp}}/\mathrm{d}y$ can be obtained by integrating (2.11),

$$\frac{\mathrm{d}\sigma_{\mathrm{pp}}^{\psi}}{\mathrm{d}y} = \int_{\vec{p}_{\perp}} \frac{\mathrm{d}\sigma_{\mathrm{pp}}^{\psi}}{\mathrm{d}y\,\mathrm{d}^2\vec{p}_{\perp}} = \mathcal{N}\int_{\vec{p}_{\perp}} \mu(p_{\perp})\,\nu(y,p_{\perp}) \simeq \mathcal{N}\left[\int_{\vec{p}_{\perp}} \mu(p_{\perp})\right]\nu(y,\bar{p}_{\perp})\,, \tag{A.5}$$

where the latter approximation arises from $\mu(p_{\perp})$ decreasing much faster than $\nu(y,p_{\perp})$ with $p_{\perp}$. This can be checked for the values of the parameters p_0, m, n (see Table 1) and within the intervals in $p_{\perp}$ and y considered in our study (see Sections 3 and 4). Comparing (A.4) and (A.5) we see that the parametrization (2.11) is consistent with that for the single differential rate (A.4) (or equivalently (A.1)) used in [19].

Let us remark that in (A.5) the typical $\bar{p}_{\perp}$ may be defined as

$$\int_0^{\bar{p}_{\perp}^2} dp_{\perp}^2\,\mu(p_{\perp}) \equiv \frac{1}{2}\int_0^{\infty} dp_{\perp}^2\,\mu(p_{\perp}) \Rightarrow \bar{p}_{\perp}^2 = \left(2^{\frac{1}{m-1}} - 1\right)p_0^2 \quad (m>1)\,. \tag{A.6}$$

Using the values of p_0 and m given in Table 1 for J/ψ, we find that $\bar{p}_{\perp}$ varies in the range $\bar{p}_{\perp}(p_0,m) = 1.3 - 2.4\,\mathrm{GeV}$, somewhat above the *ad hoc* value $\bar{p}_{\perp} = 1\,\mathrm{GeV}$ used in [19]. However, taking $\bar{p}_{\perp} \simeq 2\,\mathrm{GeV}$ instead of $1\,\mathrm{GeV}$ affects only slightly the value of $M_{\perp}$ ($M_{\perp} \simeq 3.6\,\mathrm{GeV}$ instead of $3.2\,\mathrm{GeV}$), with no sizeable effect on the predictions presented in Ref. [19].

B Effective path length vs. centrality class

In this Appendix we explain how the numbers of Table 2 in Section 2.5 have been obtained.

B.1 Number of participants and binary collisions for a given centrality class

p–A collisions (LHC case)

In the Glauber model, at a given impact parameter $\mathbf{b}$ the number of participating nucleons N_{p} in the target nucleus follows a binomial distribution,

$$P(N_{\mathrm{p}}) = \frac{\int \mathrm{d}\mathbf{b} \binom{A}{N_{\mathrm{p}}} [p_{\mathrm{pA}}(\mathbf{b})]^{N_{\mathrm{p}}} [1 - p_{\mathrm{pA}}(\mathbf{b})]^{A - N_{\mathrm{p}}}}{\int \mathrm{d}\mathbf{b} \left\{ 1 - [1 - p_{\mathrm{pA}}(\mathbf{b})]^{A} \right\}}. \tag{B.1}$$

Here $p_{\mathrm{pA}}(\mathbf{b}) \equiv \sigma_{\mathrm{in}}^{\mathrm{NN}} T_{\mathrm{A}}(\mathbf{b})$ is the probability for an inelastic collision between the projectile proton and a nucleon of the target nucleus, and $\sigma_{\mathrm{in}}^{\mathrm{NN}}$ is the inelastic p–p cross section which we take to be 70 mb at LHC energies. The target nucleus optical thickness $T_{\mathrm{A}}(\mathbf{b})$ is normalized as $\int \mathrm{d}\mathbf{b}\, T_{\mathrm{A}}(\mathbf{b}) = 1$. The denominator in (B.1) is the p–A total inelastic cross section $\sigma_{\mathrm{in}}^{\mathrm{pA}}$ and ensures the correct normalization $P(N_{\mathrm{p}} > 0) = 1$ for the total interaction probability.

The number of binary collisions coincides with the number of participating nucleons of the target.

d–A collisions (RHIC case)

The generalization of Eq. (B.1) to the d–A case is straightforward,

$$P(N_{\mathrm{p}}) = \frac{\int \mathrm{d}\mathbf{b} \int \mathrm{d}\mathbf{r} P_{\mathrm{d}}(\mathbf{r}) \binom{A}{N_{\mathrm{p}}} [p_{\mathrm{dA}}(\mathbf{b}, \mathbf{r})]^{N_{\mathrm{p}}} [1 - p_{\mathrm{dA}}(\mathbf{b}, \mathbf{r})]^{A - N_{\mathrm{p}}}}{\int \mathrm{d}\mathbf{b} \int \mathrm{d}\mathbf{r} P_{\mathrm{d}}(\mathbf{r}) \left\{ 1 - [1 - p_{\mathrm{dA}}(\mathbf{b}, \mathbf{r})]^{A} \right\}}, \tag{B.2}$$

and is obtained by introducing the distribution $P_{\mathrm{d}}(\mathbf{r})$ for the p–n transverse separation $\mathbf{r}$ in deuterium, and replacing $p_{\mathrm{pA}}(\mathbf{b})$ by the interaction probability $p_{\mathrm{dA}}(\mathbf{b}, \mathbf{r})$ of a target nucleon with either nucleon of the deuterium projectile, given by

$$p_{\mathrm{dA}}(\mathbf{b}, \mathbf{r}) \equiv \sigma_{\mathrm{in}}^{\mathrm{NN}} T_{\mathrm{A}}(\mathbf{b} + \tfrac{\mathbf{r}}{2}) + \sigma_{\mathrm{in}}^{\mathrm{NN}} T_{\mathrm{A}}(\mathbf{b} - \tfrac{\mathbf{r}}{2}) - p_2(\mathbf{b}, \mathbf{r}). \tag{B.3}$$

Here

$$p_2(\mathbf{b}, \mathbf{r}) \equiv \int \mathrm{d}\mathbf{s}\, T_{\mathrm{A}}(\mathbf{s}) p(\mathbf{b} + \mathbf{r}/2 - \mathbf{s}) p(\mathbf{b} - \mathbf{r}/2 - \mathbf{s}) \simeq T_{\mathrm{A}}(\mathbf{b}) \int \mathrm{d}\mathbf{s}\, p(\mathbf{r} + \mathbf{s}) p(\mathbf{s}) \tag{B.4}$$

is the collision probability of a target nucleon with both nucleons of the deuterium projectile. The denominator of (B.2) is the d–A total inelastic cross section $\sigma_{\mathrm{in}}^{\mathrm{dA}}$.

The probability (B.4) depends on the N–N inelastic collision probability as a function of the impact parameter $p(\mathbf{s})$. For that profile at c.m. energy $\sqrt{s} = 200$ GeV we take the Regge-inspired parametrization $p(\mathbf{b}) = 1 - \exp(-2N e^{-\mathbf{b}^2/\alpha})$ with $\alpha = 1.05$ fm^2 and $N = 1.1$, giving the total p–p inelastic cross section $\sigma_{\mathrm{in}}^{\mathrm{NN}} = \int \mathrm{d}\mathbf{s}\, p(\mathbf{s}) = 4.2\,\mathrm{fm}^2 = 42\,\mathrm{mb}$. The distribution $P_{\mathrm{d}}(\mathbf{r})$ is evaluated by assuming a Hulthen form for the deuterium wave

function. The thickness functions of all target nuclei considered in our study (Be, Fe, W, Au, Pb) are extracted from low-energy electron–proton scattering experiments [31].

Summing up the probabilities (B.1) and (B.2) we find the threshold values $N_p^{\min}$ and $N_p^{\max}$ which saturate approximately 20% of the total interaction probability $P(N_p \geq 1) = 1$, as described in Section 2.5.

In the d–A case, the number of binary collisions differs from N_p by the number of target nucleons which undergo collisions with both nucleons of the deuterium projectile:

$$\langle \Delta N \rangle|_{N \in [N_1, N_2]} = \frac{\sum\limits_{N=N_1}^{N_2} N \binom{A}{N} \int d\mathbf{b} \int d\mathbf{r} P_d(\mathbf{r}) p_2(\mathbf{b}, \mathbf{r}) \left[p_{dA}(\mathbf{b}, \mathbf{r}) \right]^{N-1} \left[1 - p_{dA}(\mathbf{b}, \mathbf{r}) \right]^{A-N}}{\sum\limits_{N=N_1}^{N_2} \binom{A}{N} \int d\mathbf{b} \int d\mathbf{r} P_d(\mathbf{r}) \left[p_{dA}(\mathbf{b}, \mathbf{r}) \right]^{N} \left[1 - p_{dA}(\mathbf{b}, \mathbf{r}) \right]^{A-N}}.$$
(B.5)

B.2 Average number of collisions in the events with a hard process

p–A (LHC case)

In the case of triggering on J/ψ production (or any other hard process with a small cross section) the average number of collisions for the participating nucleon gets modified. The hard production process can occur in each of the inelastic collisions of the projectile nucleon with a probability $\sigma_{J/\psi}/\sigma_{\mathrm{in}}^{NN}$,[12] so that the hard process probability is $P(J/\psi|N_p) = N_p \, \sigma_{J/\psi}/\sigma_{\mathrm{in}}^{NN}$ and the joint probability for the hard production and N_p participating nucleons in the target is

$$P(N_p, J/\psi) = \frac{N_p}{\sigma_{\mathrm{in}}^{pA}} \frac{\sigma_{J/\psi}}{\sigma_{\mathrm{in}}^{NN}} \int d\mathbf{b} \binom{A}{N_p} \left[p_{pA}(\mathbf{b}) \right]^{N_p} \left[1 - p_{pA}(\mathbf{b}) \right]^{A-N_p}.$$
(B.6)

The normalized probability distribution for the number of collisions of the projectile proton in the events tagged by both centrality and J/ψ production is

$$P(N_p | J/\psi, [N_1, N_2]) = \frac{\frac{\sigma_{J/\psi}}{\sigma_{\mathrm{in}}^{NN}} N_p \int d\mathbf{b} \binom{A}{N_p} \left[p_{pA}(\mathbf{b}) \right]^{N_p} \left[1 - p_{pA}(\mathbf{b}) \right]^{A-N_p}}{\sum\limits_{N=N_1}^{N_2} \frac{\sigma_{J/\psi}}{\sigma_{\mathrm{in}}^{NN}} N \int d\mathbf{b} \binom{A}{N} \left[p_{pA}(\mathbf{b}) \right]^{N} \left[1 - p_{pA}(\mathbf{b}) \right]^{A-N}}$$
(B.7)

and is independent of the hard process cross section. The corresponding average of N_p is

$$\langle N_p \rangle|_{J/\psi, [N_1, N_2]} = 1 + \frac{\sum\limits_{N=N_1}^{N_2} N(N-1) \int d\mathbf{b} \binom{A}{N} \left[p_{pA}(\mathbf{b}) \right]^{N} \left[1 - p_{pA}(\mathbf{b}) \right]^{A-N}}{\sum\limits_{N=N_1}^{N_2} N \int d\mathbf{b} \binom{A}{N} \left[p_{pA}(\mathbf{b}) \right]^{N} \left[1 - p_{pA}(\mathbf{b}) \right]^{A-N}}.$$
(B.8)

The interpretation of (B.8) is straightforward. Unity stands for the target nucleon which participated to the hard process. The second term corresponds to the target nucleons

---

[12]We assume that the hard process cross section is small, so that the probability of two hard processes in the same p–A collision can be neglected.

which also undergo an inelastic collision with the projectile, and may thus contribute to the transverse momentum broadening of the $c\bar{c}$ pair, with the probability $\sigma_{broad}/\sigma_{in}^{NN}$.

The effective path length in the target nucleus for the centrality class $[N_1, N_2]$ thus reads

$$L_A = L_p + \frac{\sum\limits_{N=N_1}^{N_2} N(N-1) \int d\mathbf{b} \binom{A}{N} [p_{pA}(\mathbf{b})]^N [1-p_{pA}(\mathbf{b})]^{A-N}}{\sigma_{in}^{NN} \rho_0 \sum\limits_{N=N_1}^{N_2} N \int d\mathbf{b} \binom{A}{N} [p_{pA}(\mathbf{b})]^N [1-p_{pA}(\mathbf{b})]^{A-N}}, \qquad (B.9)$$

where L_p is the corresponding length in a proton target. For the minimum bias case doing the summations is trivial and one recovers the expression used in Ref. [19]. In the numerical applications we take $L_p = 1.5\,\mathrm{fm}$ and $\rho_0 = 0.17\,\mathrm{fm}^{-3}$.

d–A (RHIC case)

Compared to the p–A case some complications arise because of the deuterium projectile. What is relevant for the broadening is the number of collisions N_t suffered by the nucleon of the deuterium participating to the hard process. This number is not equal to the number of participants in a given event. In the binomial expansion of the first multiplier in the numerator of (B.2)

$$[p_{dA}(\mathbf{b}, \mathbf{r})]^{N_p} = \binom{N_p}{N_t} [p_{pA}(\mathbf{b}+\mathbf{r}/2)]^{N_t} [p_{pA}(\mathbf{b}-\mathbf{r}/2) - p_2(\mathbf{b}, \mathbf{r})]^{N_p - N_t}, \qquad (B.10)$$

each term corresponds to the probability of N_t collisions of the tagged nucleon of the deuterium projectile with overall N_p participants in the target nucleus. The joint probability of the production process in d–A collision with given N_t and overall N_p thus reads:

$$P(N_p, N_t, J/\psi) = \frac{2N_t}{\sigma_{in}^{dA}} \frac{\sigma_{J/\psi}}{\sigma_{in}^{NN}} \int d\mathbf{b} \int d\mathbf{r} P_d(\mathbf{r}) \times$$
$$\binom{A}{N_p} \binom{N_p}{N_t} [p_{pA}(\mathbf{b}+\mathbf{r}/2)]^{N_t} [p_{pA}(\mathbf{b}-\mathbf{r}/2) - p_2(\mathbf{b}, \mathbf{r})]^{N_p - N_t} [1 - p_{dA}(\mathbf{b}, \mathbf{r})]^{A-N_p}. \quad (B.11)$$

Correspondingly the number of inelastic rescatterings for the nucleon of the deuterium projectile tagged by the hard process is

$$\langle N_t \rangle |_{J/\psi,[N_1,N_2]} = 1+$$
$$\frac{\sum\limits_{N=N_1}^{N_2} N(N-1) \int d\mathbf{b} \int d\mathbf{r} P_d(\mathbf{r}) \binom{A}{N} [p_{pA}(\mathbf{b})]^2 [p_{dA}(\mathbf{b}, \mathbf{r})]^{N-2} [1-p_{dA}(\mathbf{b}, \mathbf{r})]^{A-N}}{\sum\limits_{N=N_1}^{N_2} N(N-1) \int d\mathbf{b} \int d\mathbf{r} P_d(\mathbf{r}) \binom{A}{N} p_{pA}(\mathbf{b}) [p_{dA}(\mathbf{b}, \mathbf{r})]^{N-1} [1-p_{dA}(\mathbf{b}, \mathbf{r})]^{A-N}} \qquad (B.12)$$

Interpretation of (B.12) goes along the same line as for (B.8).

The path length of the $c\bar{c}$ pair for a given centrality class is thus (after substituting $p_{\mathrm{pA}}(\mathbf{b}) = \sigma_{\mathrm{in}}^{\mathrm{NN}} T_{\mathrm{A}}(\mathbf{b})$):

$$L_{\mathrm{A}} = L_{\mathrm{p}} + \frac{\sum\limits_{N=N_1}^{N_2} N(N-1) \int \mathrm{d}\mathbf{b} \int \mathrm{d}\mathbf{r} P_{\mathrm{d}}(\mathbf{r}) \binom{A}{N} (T_A(\mathbf{b}))^2 \left[p_{\mathrm{dA}}(\mathbf{b}, \mathbf{r})\right]^{N-2} \left[1 - p_{\mathrm{dA}}(\mathbf{b}, \mathbf{r})\right]^{A-N}}{\rho_0 \sum\limits_{N=N_1}^{N_2} N(N-1) \int \mathrm{d}\mathbf{b} \int \mathrm{d}\mathbf{r} P_{\mathrm{d}}(\mathbf{r}) \binom{A}{N} T_A(\mathbf{b}) \left[p_{\mathrm{dA}}(\mathbf{b}, \mathbf{r})\right]^{N-1} \left[1 - p_{\mathrm{dA}}(\mathbf{b}, \mathbf{r})\right]^{A-N}}$$

(B.13)

For the minimum bias case ($N_1 = 1$, $N_2 = A$) the summations in (B.13) are explicit and one again recovers the expression (3.18) of Ref. [19]. The path length for the different centrality classes is given in Table 2.

References

[1] **PHENIX** collaboration, S. S. Adler et al., *Suppressed π^0 production at large transverse momentum in central Au + Au collisions at $\sqrt{s}$ = 200 GeV*, Phys. Rev. Lett. **91** (2003) 072301, [`nucl-ex/0304022`].

[2] **STAR** collaboration, J. Adams et al., *Transverse momentum and collision energy dependence of high p_T hadron suppression in Au + Au collisions at ultrarelativistic energies*, Phys. Rev. Lett. **91** (2003) 172302, [`nucl-ex/0305015`].

[3] **ALICE** collaboration, K. Aamodt et al., *Suppression of Charged Particle Production at Large Transverse Momentum in Central Pb–Pb Collisions at $\sqrt{s_{NN}}$ = 2.76 TeV*, Phys. Lett. **B696** (2011) 30, [`arXiv:1012.1004`].

[4] **CMS** collaboration, S. Chatrchyan et al., *Study of high-p_T charged particle suppression in Pb–Pb compared to p–p collisions at $\sqrt{s_{\mathrm{NN}}}$ =2.76 TeV*, Eur. Phys. J. **C72** (2012) 1945, [`arXiv:1202.2554`].

[5] **ATLAS** collaboration, G. Aad et al., *Observation of a Centrality-Dependent Dijet Asymmetry in Lead-Lead Collisions at $\sqrt{s_{NN}}$ = 2.77 TeV with the ATLAS Detector at the LHC*, Phys.Rev.Lett. **105** (2010) 252303, [`arXiv:1011.6182`].

[6] **CMS** collaboration, S. Chatrchyan et al., *Jet momentum dependence of jet quenching in PbPb collisions at $\sqrt{s_{NN}}$ = 2.76 TeV*, Phys.Lett. **B712** (2012) 176–197, [`arXiv:1202.5022`].

[7] D. d'Enterria, *Jet quenching, Springer Verlag. Landolt-Boernstein Vol. 1-23A* (2009) [`arXiv:0902.2011`].

[8] T. Matsui and H. Satz, *J/ψ suppression by Quark–Gluon plasma formation*, Phys. Lett. **B178** (1986) 416.

[9] A. D. Frawley, T. Ullrich, and R. Vogt, *Heavy flavor in heavy-ion collisions at RHIC and RHIC II*, Phys. Rept. **462** (2008) 125, [`arXiv:0806.1013`].

[10] **BRAHMS** collaboration, I. Arsene et al., *On the evolution of the nuclear modification factors with rapidity and centrality in d + Au collisions at $\sqrt{s_{\mathrm{NN}}}$ =200 GeV*, Phys. Rev. Lett. **93** (2004) 242303, [`nucl-ex/0403005`].

[11] **PHENIX** collaboration, S. Adler et al., *Nuclear modification factors for hadrons at forward and backward rapidities in deuteron-gold collisions at $\sqrt{s_{\mathrm{NN}}}$ =200 GeV*, Phys. Rev. Lett. **94** (2005) 082302, [`nucl-ex/0411054`].

[12] **FNAL E866/NuSea** collaboration, M. J. Leitch et al., *Measurement of Differences between J/ψ and ψ′ Suppression in p–A Collisions*, *Phys. Rev. Lett.* **84** (2000) 3256, [`nucl-ex/9909007`].

[13] **PHENIX** collaboration, A. Adare, S. Afanasiev, C. Aidala, N. Ajitanand, Y. Akiba, et al., *Transverse-Momentum Dependence of the J/ψ Nuclear Modification in d–Au Collisions at* $\sqrt{s_{\mathrm{NN}}} = 200$ *GeV*, [`arXiv:1204.0777`].

[14] B. Kopeliovich, I. Potashnikova, and I. Schmidt, *Nuclear suppression of J/Psi: from RHIC to the LHC*, *Nucl.Phys.* **A864** (2011) 203–212, [`arXiv:1012.5648`].

[15] E. Ferreiro, F. Fleuret, J. Lansberg, N. Matagne, and A. Rakotozafindrabe, *Centrality, Rapidity, and Transverse-Momentum Dependence of Gluon Shadowing and Antishadowing on J/ψ Production in dAu Collisions at* $\sqrt{s}$=200 *GeV*, *Few Body Syst.* **53** (2012) 27–36, [`arXiv:1201.5574`].

[16] C. J. Benesh, J. Qiu, and J. P. Vary, *J/ψ suppression in hadron-nucleus collisions*, *Phys.Rev.* **C50** (1994) 1015–1023, [`hep-ph/9403265`].

[17] H. Fujii, F. Gelis, and R. Venugopalan, *Quark pair production in high energy pA collisions: General features*, *Nucl. Phys.* **A780** (2006) 146, [`hep-ph/0603099`].

[18] R. Sharma and I. Vitev, *High transverse momentum quarkonium production and dissociation in heavy ion collisions*, [`arXiv:1203.0329`].

[19] F. Arleo and S. Peigné, *Heavy-quarkonium suppression in p-A collisions from parton energy loss in cold QCD matter*, *JHEP* **03** (2013) 122, [`arXiv:1212.0434`].

[20] F. Arleo and S. Peigné, *J/ψ suppression in p-A collisions from parton energy loss in cold QCD matter*, *Phys. Rev. Lett.* **109** (2012) 122301, [`arXiv:1204.4609`].

[21] F. Arleo, S. Peigné, and T. Sami, *Revisiting scaling properties of medium-induced gluon radiation*, *Phys. Rev.* **D83** (2011) 114036, [`arXiv:1006.0818`].

[22] R. Neufeld, I. Vitev, and B.-W. Zhang, *A possible determination of the quark radiation length in cold nuclear matter*, *Phys.Lett.* **B704** (2011) 590, [`arXiv:1010.3708`].

[23] **ALICE** collaboration, K. Aamodt et al., *Rapidity and transverse momentum dependence of inclusive J/ψ production in pp collisions at* $\sqrt{s} = 7$ *TeV*, *Phys. Lett.* **B704** (2011) 442, [`arXiv:1105.0380`].

[24] **ATLAS** collaboration, G. Aad et al., *Measurement of the differential cross-sections of inclusive, prompt and non-prompt J/ψ production in proton-proton collisions at* $\sqrt{s} = 7$ *TeV*, *Nucl.Phys.* **B850** (2011) 387–444, [`arXiv:1104.3038`].

[25] **LHCb** collaboration, R. Aaij et al., *Measurement of J/ψ production in pp collisions at* $\sqrt{s} = 7$ TeV, *Eur.Phys.J.* **C71** (2011) 1645, [`arXiv:1103.0423`].

[26] **LHCb** collaboration, et al., *Measurement of Υ production in p–p collisions at* $\sqrt{s} = 7$ *TeV*, *Eur. Phys. J.* **C72** (2012) 2025, [`arXiv:1202.6579`].

[27] **PHENIX** collaboration, A. Adare et al., *J/ψ production versus transverse momentum and rapidity in* $p^{+}p$ *collisions at* $\sqrt{s} = 200$ *GeV*, *Phys. Rev. Lett.* **98** (2007) 232002, [`hep-ex/0611020`].

[28] **E789** collaboration, M. H. Schub et al., *Measurement of J/ψ and ψ′ production in 800 GeV/c proton - gold collisions*, *Phys. Rev.* **D52** (1995) 1307.

[29] **PHENIX** collaboration, S. Adler et al., *Centrality dependence of charged hadron production in deuteron + gold and nucleon + gold collisions at s(NN)**(1/2) = 200-GeV*, Phys.Rev. **C77** (2008) 014905, [arXiv:0708.2416].

[30] **ALICE** collaboration, B. Abelev et al., *Long-range angular correlations on the near and away side in p-Pb collisions at $\sqrt{s_{NN}} = 5.02$ TeV*, Phys.Lett. **B719** (2013) 29–41, [arXiv:1212.2001].

[31] C. W. De Jager, H. De Vries, and C. De Vries, *Nuclear charge and magnetization density distribution parameters from elastic electron scattering*, Atom. Data Nucl. Data Tabl. **36** (1987) 495.